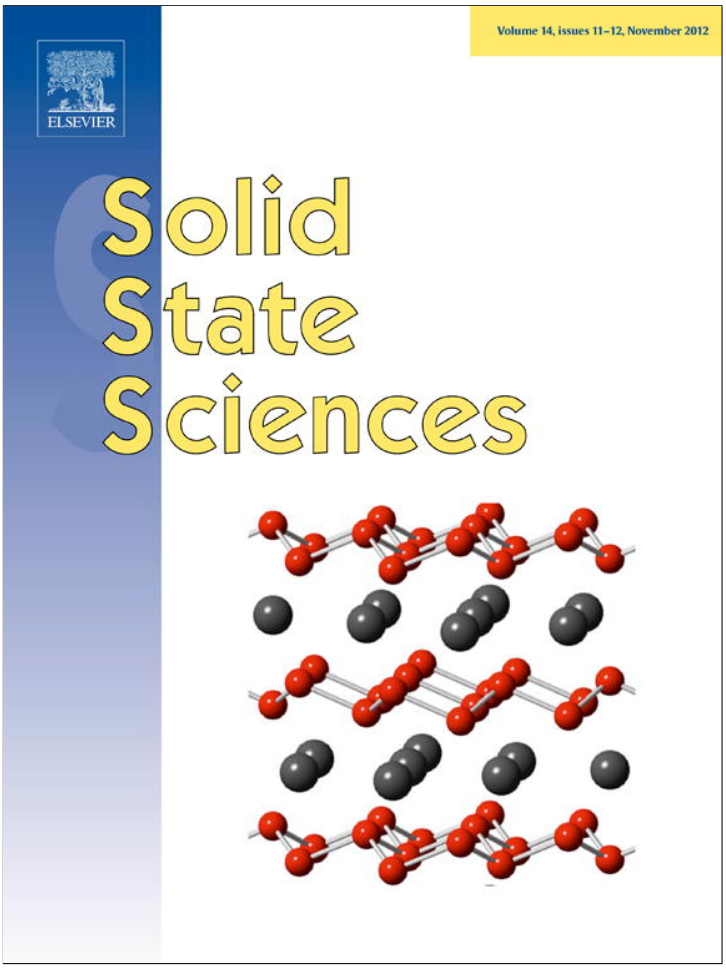

Solid State Sciences 14 (2012) 1648–1652

Contents lists available at SciVerse ScienceDirect

Solid State Sciences

journal homepage: www.elsevier.com/locate/ssscie

Prediction of orientational phase transition in boron carbide

M. Widom*, W.P. Huhn

Department of Physics, Carnegie Mellon University, 5000 Forbes Ave, Pittsburgh, PA 15232, United States

ARTICLE INFO

Article history:
Received 2 November 2011
Received in revised form
18 April 2012
Accepted 17 May 2012
Available online 26 May 2012

Keywords:
Boron carbide
B_4C
$B_{13}C_2$
Phase diagram
Orientational phase transition
Density functional theory

ABSTRACT

The assessed binary phase diagram of boron–carbon exhibits a single intrinsically disordered alloy phase designated "B_4C" with rhombohedral symmetry occupying a broad composition range that falls just short of the nominal carbon content of 20%. As this composition range is nearly temperature independent, the phase diagram suggests a violation of the third law of thermodynamics, which typically requires compounds to achieve a definite stoichiometry at low temperatures. By means of first principles total energy calculations we predict the existence of two stoichiometric phases at $T = 0$ K: one of composition B_4C with monoclinic symmetry; the other of composition $B_{13}C_2$ with rhombohedral symmetry. Using statistical mechanics to extend to finite temperatures, we demonstrate that the monoclinic phase reverts to the observed disordered nonstoichiometric rhombohedral phase above $T = 600$ K, along with a slight reduction on carbon content.

1. Introduction

Only a single compound is reported in the boron–carbon binary system, the nonstoichiometric compound boron carbide, often named "B_4C" whose composition range extends from 9 to 19.2% carbon. Notice this range excludes the 20% carbon that is expected for the implied stoichiometry of B_4C. Presumably the composition range is due to substitutional disorder between B and C atoms. As commonly drawn, the composition range is nearly independent of temperature over the range 1000–2000° C (1273–2273 K) [1,2]. If this composition range were to persist at low temperatures it would imply the existence of substitutional disorder, and hence configurational entropy, at $T = 0$ K, in apparent violation of the third law of thermodynamics [3,4]. Other phase diagrams have been proposed but rejected, including one [5,6] containing a large number of distinct phases, one of which is labeled $B_{13}C_2$ with variable stoichiometry at high temperature but reaches a fixed stoichiometry as T approaches 0 K.

Boron carbide displays rhombohedral symmetry (space group $R\bar{3}m$, #166), based on a 15 atom primitive cell (Pearson symbol hR15). Its structure is similar to α-boron (Pearson hR12), which places 12-atom icosahedra at vertices of the rhombohedron, but boron carbide includes an additional chain of three atoms in the center of the rhombohedral cell aligned along the 3-fold axis (see Fig. 1). The symmetry of the structure depends on the placement of chemical species B and C among these sites. Maintaining full boron occupancy (B_{12}) of the icosahedron and placing a C–B–C chain along the axis results in a rhombohedral structure [7] of composition $B_{13}C_2$ (carbon fraction $x_C = 0.133$). Such a structure have been reported experimentally [8,9], although given the substitutional disorder between B and C it is preferable to assign occupation probabilities to each site [10].

At composition $B_{12}C_3 = B_4C$, rhombohedral symmetry is maintained with a B_{12} icosahedron and a C–C–C chain [7,11,12]. However, first principles calculations [13,14] suggest total energy is reduced by substituting carbon for one icosahedral boron atom at the "polar" position indicated in Fig. 1 (right). The symmetry breaking caused by the chemical substitution of carbon onto the icosahedron reduces the symmetry from rhombohedral to monoclinic, yielding Pearson type mC30 (space group *Cm*, #8).

The higher rhombohedral symmetry can be restored, at any carbon content, by randomly substituting carbon among all six polar icosahedral positions with equal weight. Indeed, experimental evidence [15] suggests the true structure is a composition-dependent mixture of structural units based on B_{12} and $B_{11}C_1$ icosahedra, and likewise a mixture of C–B–C, C–B–B and B–V–B chains (V = vacancy).

We carry out first principles total energy calculations to study the distribution of carbon and boron atoms on the underlying hR15 crystal structure. The immediate output of our calculations is

* Corresponding author. Tel.: +1 412 268 7645.
E-mail addresses: widom@andrew.cmu.edu (M. Widom), wph@andrew.cmu.edu (W.P. Huhn).

1293-2558/$ – see front matter © 2012 Elsevier Masson SAS. All rights reserved.
doi:10.1016/j.solidstatesciences.2012.05.010

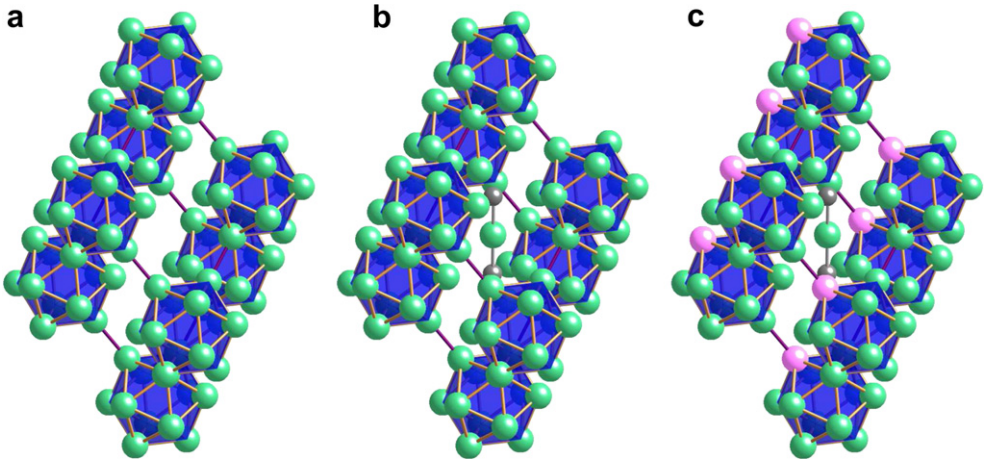

Fig. 1. (a) α-Boron (hR12); (b) $B_{13}C_2$ (hR15); (c) B_4C (mC30). Boron atoms in green, carbon in gray. Pink atom labels "polar" carbon site. (For interpretation of the references to colour in this figure legend, the reader is referred to the web version of this article.)

a predicted phase diagram in the limit of $T = 0$ K that reveals two stable well-ordered stoichiometric compounds, precisely the $B_{13}C_2$ and B_4C structures illustrated in Fig. 1. Identical conclusions were previously reached by Bylander and Kleinman [16] and by Vast et al. [17]. However, we explore the ensemble of higher energy structures obtained by varying the placement of carbon atoms among the sites, both of the 15 atom primitive cell and of various supercell. We then calculate the configurational partition function in order to obtain the finite temperature free energy. Our calculational methods are discussed in the following section.

This free energy predicts that the B_4C phase is unstable above $T = 600$ K. The principle excitation that destabilizes the B_4C phase corresponds to independent rotations of the $B_{11}C_1$ icosahedra in adjoining primitive cells, resulting in a restoration of full rhombohedral symmetry. A secondary effect is the replacement of polar carbons with boron, causing a slight reduction in the carbon content below the ideal B_4C stoichiometry. Because the $B_{13}C_2$ phase already has rhombohedral symmetry, it suffers no phase change as temperature rises, until melting around $T = 2800$ K. However, the composition of "$B_{13}C_2$" becomes highly variable as temperature rises. Indeed, the high temperature limit of the phase termed "B_4C" should properly be considered as the "$B_{13}C_2$" phase at a high C content.

Note the confusion that arises from naming phases according to their approximate stoichiometry. We advocate that the phases should be referred to by their symmetry, as implied by Landau theory. Henceforth we shall refer to the "rhombohedral phase", whose composition centers around $B_{13}C_2$ but ranges from a low of 9% C to a high of almost 20%, and the "monoclinic phase", whose composition lies in the vicinity of B_4C.

2. Theory/calculations

2.1. First principles total energy calculations

First principles total energy calculations yield the enthalpy of formation of specific trial structures. Enthalpy minima, i.e. the convex hull of $H(x)$ where x is composition, correspond to predicted low temperature stable phases. Structures lying above the convex hull are unstable to decomposition into competing stable phases at low temperature, but they can contribute significantly to the free energy at elevated temperatures as outlined in the following section.

Our total energy calculations are based on electronic density functional theory, the highest level of theory presently available for extended structures. We utilize projector augmented wave (PAW) potentials [18], an all-electron generalization of pseudopotentials, as implemented in the plane wave code VASP [19,20]. For our exchange correlation potential we choose the PW91 generalized gradient approximation (GGA) [21]. All structures are fully relaxed in both atomic and cell coordinates, yielding enthalpy H_i for structure i at $T = P = 0$. Default energy cutoffs of 400 eV were used for plane wave calculations. Brillouin zone integrations were performed using Monkhorst–Pack k-point meshes [22] sufficiently dense that energies converged to within 0.001 eV/atom. We subtract all enthalpies from the tie-line connecting elemental boron (β-boron, Pearson hR141 optimized with 107 atoms [23]) with elemental carbon (graphite, Pearson hP4), yielding the enthalpy of formation ΔH_i. We also define the energy of instability, ΔE_i, as the energy of an unstable structure above the tie-lines joining competing stable phases on the convex hull of $H(x)$.

In order to fully explore configuration space we carry out calculations both in the primitive cell and in supercell, including a $2 \times 1 \times 1$ cell doubled along the rhombohedral a axis, the hexagonal unit cell formed from three primitive cells, and a $2 \times 2 \times 1$ supercell doubled along both the a and b rhombohedral axes, containing four primitive cells. The use of supercells is demanded by the computational requirement of periodic boundary conditions. We do not believe that boron carbide actually exhibits superlattice ordering. Rather, we use a sequence of supercells of increasing size to converge toward the thermodynamic limit of infinitely many cells, with structural units containing possibly different arrangements of B and C atoms within each.

We concentrate our efforts on structures expected to be low in energy based on results from the primitive cell calculations. For the primitive cell, we used all possible symmetry independent primitive cell configurations up to 27% carbon concentration. In supercells we explored many (but not all) of the possible combinations of primitive cell configurations. The vast majority of combinations yield high energy. Configurations containing the well-known structure elements of B_{12}, $B_{11}C_1$, and $B_{10}C_2$ icosahedra, and containing C–B–C and C–B–B chains prove reasonably low in energy. The combination of a $B_{10}C_2$ icosahedron with a B_{12} icosahedron forms the bipolar defect [24]. All possible positions of carbon atoms within each icosahedron and chain are considered. Structures are grouped into symmetry-equivalent classes and we record their multiplicities, that is, the number of distinct symmetry-equivalent structures. Enthalpies of selected structures are shown in Fig. 2 for each cell size considered, and listed in Table 1 for the hexagonal unit cell.

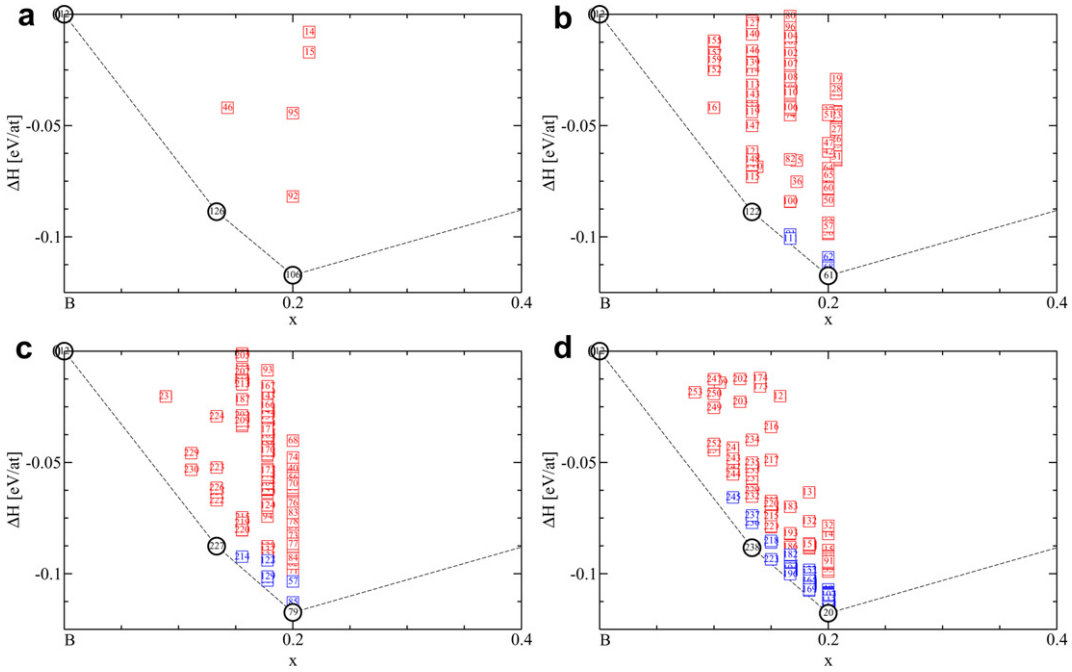

Fig. 2. Cohesive energies of boron carbide structures, left to right, top to bottom: (a) 15 atom primitive cell; (b) 30 atom $2 \times 1 \times 1$ supercell; (c) 45 atom hexagonal unit cell; (d) 60 atoms $2 \times 2 \times 1$ supercell. Heavy black circles at $x_C = 0.133$ and 0.20, respectively, correspond to the ideal $B_{13}C_2$ and B_4C structures displayed in Fig. 1. Data points in blue have $0 < \Delta E < 0.015$ eV/atom, while red has 0.015 eV/atom $< \Delta E$. (For interpretation of the references to colour in this figure legend, the reader is referred to the web version of this article.)

2.2. Configurational free energy

To go from the total energy of a configuration of $N = N_B + N_C$ atoms $E(\{r_j\})$ in volume V to the free energy, we must calculate the statistical mechanical partition function

$$Z(N_B, N_C, V, T) = \int_V \Pi_j dr_j e^{-E(\{r_j\})/(k_B T)}$$

However, we prefer to work at fixed pressure, hence we switch to the Gibbs (N,P,T) ensemble,

$$Q(N_B, N_C, P, T) = \int dV e^{-PV/(k_B T)} Z(N_B, N_C, V, T)$$

Since the dominant contributions to the partition function arise at relatively low energies, we can replace the integral over positions $\{r_j\}$ and volumes V with a sum over local energy minima of a Boltzmann-like factor $e^{-F_{vib}^{(i)}/(k_B T)}$ related to the vibrational free energy of the local minimum i,

$$Q(N_B, N_C, P, T) \approx \sum_i e^{-F_{vib}^{(i)}/(k_B T)}$$

As a further approximation, we replace $F_{vib}^{(i)}$ with the enthalpy ΔH_i. While this assumption is certainly not valid, the result should affect our conclusions only quantitatively, not qualitatively, provided the vibrational properties of different relaxed configurations differ only slightly. Only discrete configurational degrees of freedom remain, corresponding the distinct distributions of B and C atoms among the atomic sites.

Taking the logarithm, we obtain the Gibbs free energy

$$G(N_B, N_C, P, T) = -k_B T \ln Q(N_B, N_C, P, T) = \mu_B N_B + \mu_C N_C.$$

Since the total number of atoms $N = N_B + N_C$ is fixed, for a given primitive cell or supercell, it is convenient to re-express $G(N_B,N_C,T) = \mu_B N + \delta\mu N_C$, where $\delta\mu = \mu_C - \mu_B$. In fact, we can change to a semi-grand canonical potential

$$\Sigma(N, \delta\mu, T) = \sum_{N_C} e^{\delta\mu N_C/(k_B T)} Q(N - N_C, N_C, T)$$

and use the chemical potential difference to control the composition $x_C = N_C/(N_B + N_C)$. The free energy in this ensemble is simply $Y(N,\delta\mu,T) = -k_B T \ln Z = \mu_B N$. Inspecting the enthalpies shown in Fig. 2 we see that choosing $\delta\mu = 0$ at low temperature places us in the monoclinic phase at $x_C = 0.200$, while $\delta\mu = -0.55$ eV/atom corresponds to the rhombohedral phase at $x_C = 0.133$.

Table 1
Table of low ΔE structures for pure elements and the hexagonal boron carbide cell. In our naming scheme, adapted from the primitive cell, sites listed are those containing carbons. t and t′ denotes the two ends of the chain (so that tt′ denotes a C–B–C chain), p{0,1,2} denotes the polar atoms on the "north" side of the icosahedra, p′{0,1,2} denotes the polar atoms on the opposite "south" side of the icosahedra. Likewise e{0,1,2} and e′{0,1,2} denotes the atoms just to the north and south of the equator. Energy units are meV/atom. Ω is the multiplicity.

Name	ΔE	ΔH	x_C	Atoms	Ω	Description
C.hP4	0	0	1	C_4	1	Graphite
B.hR141	0	0	0	B_{107}	1	β Boron
(p0tt′)(p0tt′)(p0tt′)	0	−117.4	0.2	$B_{36}C_9$	6	B_4C (monoclinic)
(tt′)(tt′)(tt′)	0	−87.6	0.133	$B_{39}C_6$	1	$B_{13}C_2$ (rhombohedral)
(p0tt′)(p0tt′)(p1tt′)	3.0	−114.4	0.2	$B_{36}C_9$	36	Rotation
(p0tt')(p0tt')(tt')	4.4	−103.1	0.178	$B_{37}C_8$	18	Mixed icosahedra
(p0tt′)(p1tt′)(p2tt′)	4.5	−112.9	0.2	$B_{36}C_9$	12	Rotation
(p0tt′)(tt′)(tt′)	5.2	−92.4	0.156	$B_{38}C_7$	18	Mixed icosahedra
(p0tt′)(p1tt′)(tt′)	6.2	−101.3	0.178	$B_{37}C_8$	36	Mixed icosahedra
(p1p1′tt′)(tt′)(p0tt′)	10.6	−106.8	0.2	$B_{36}C_9$	36	Bipolar defect
(p0tt′)(p1′tt′)(tt′)	13.4	−94.0	0.178	$B_{37}C_8$	18	Mixed icosahedra
(e0tt′)(p0′tt′)(p0tt′)	13.9	−103.5	0.2	$B_{36}C_9$	18	One equatorial, rotation

3. Results and discussion

Differentiating Y with respect to $\delta\mu$ gives the number of carbon atoms N_C, while two derivatives with respect to T give the heat capacity due to the discrete configurational degrees of freedom

$$C_P(N,\delta\mu,T) = T\frac{d^2Y}{dT^2} = -k_BT\frac{d^2(TlnZ)}{dT^2} = \frac{<H^2>-<H>^2}{k_BT^2}$$

where angle brackets indicate the configurational ensemble average, and H is the enthalpy of formation. Results for C_P are shown in Fig. 3, using the energies displayed in Fig. 2. Note that we only use subsets of the possible energies (those in black and blue), chosen to accurately reflect the thermodynamics up to $T = 1000$ K but omitting higher energy states that would cause the heat capacity to rise again as T increases. These states were omitted for reasons of limitations in computer time when dealing with larger cells and have no impact on the curves shown in Fig. 3.

A phase transition is clearly indicated at $\delta\mu = 0$ by the peak in heat capacity around $T = 500$–600 K. The peak is growing in strength as system size increases, indicating a divergence in the infinite size limit. The peak is entirely absent in the case of the single primitive cell because the relevant excitation, rotations of C among polar B sites, is an exact symmetry of the primitive cell. In fact, there is a 6-fold degeneracy of the ground state. This degeneracy has no consequence in the thermodynamic limit as it is nonextensive. A weak peak is observed around $T = 100$–200 K in the two even supercells (30 and 60 atoms). These are due to a loss of inversion symmetry but with non-extensive multiplicity, so that the peak height tends to zero in the thermodynamic limit. For super cells of two or more primitive cells, the primary peak corresponds to rotation of the carbon atoms among icosahedral polar sites. The relevant excitations are rotational degrees of freedom in the selection of polar site on which to place carbon atoms. Because this phase transition corresponds to unlocking the orientations of polar carbons, rhombohedral symmetry is restored in the high temperature phase.

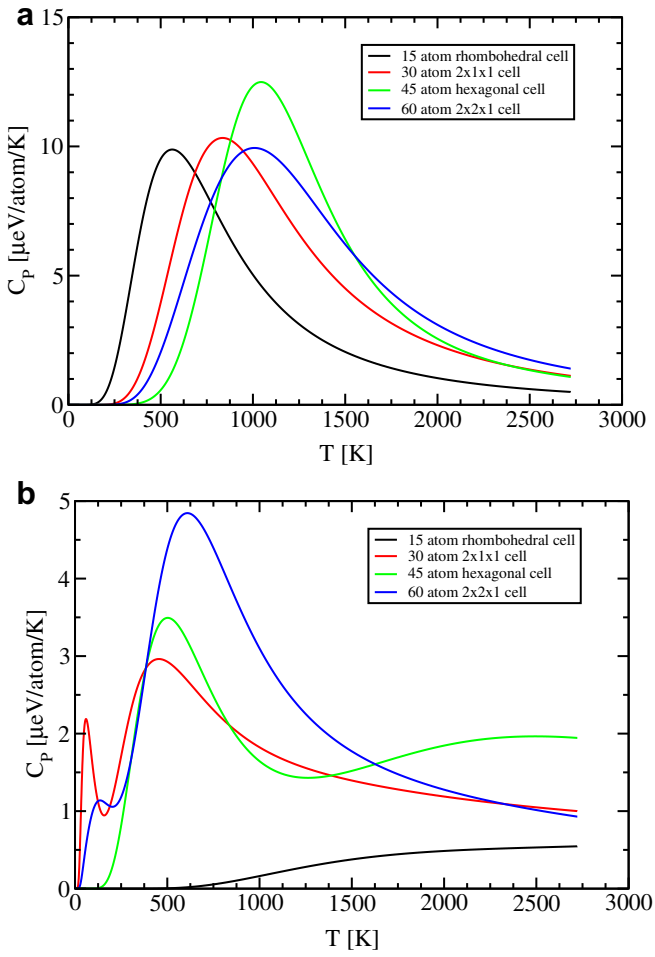

Fig. 3. Heat capacity at (a) $\delta\mu = -0.55$, and (b) $\delta\mu = 0$.

Although there is a heat capacity peak at $\delta\mu = -0.55$, this peak does not grow in magnitude as system size increases, and thus is not an evidence of a phase transition. It is caused by excitation of $B_{11}C_1$ icosahedra, of random orientations, while only B_{12} exist in the ground state at this chemical potential. Thus the rhombohedral phase persists to high temperature with no change in thermodynamic state. The presence of polar carbons as low energy excitations allows this phase to exhibit a broad composition range. Owing to orientational disorder, full rhombohedral symmetry is present throughout the entire temperature and composition range.

By varying the chemical potential $\delta\mu$ we may vary the compositions of the rhombohedral and monoclinic phases. We find that the monoclinic composition remains nearly fixed at $x_C = 1/5 = 0.200$ at low temperatures. The rhombohedral composition shows some variability around the value $x_C = 2/15 = 0.133$ at low temperature, and high variability at high temperatures, reaching a low value of $x_C = 0.070$ a high value of $x_C = 0.198$. We do not expect our low carbon limit to be accurate because we have not extensively studied boron-rich structures. The carbon content decreases at high temperature owing to the entropy of selecting icosahedra on which to replace polar carbon atoms with boron. The high temperature limit at $\delta\mu = 0$ is precisely the same thermodynamic phase as was obtained at $\delta\mu = -0.55$.

4. Conclusions

In conclusion, our first principles calculations predict the existence of two distinct boron carbide phases with differing symmetries at low temperatures. One has precise stoichiometry $B_{13}C_2$ and rhombohedral symmetry. The other has precise stoichiometry B_4C and monoclinic symmetry. At high temperatures the monoclinic B_4C phase undergoes an orientational disordering transition and becomes thermodynamically indistinct from the rhombohedral $B_{13}C_2$ phase. The high temperature phase is thus predicted to be a highly disordered mixture of icosahedra and chains of varying B–C occupancy.

Experimental verification of this proposal will be difficult, if not impossible, owing to the very long equilibration times expected at the low temperatures where the monoclinic phase is stable. The mechanism to produce the orientationally ordered monoclinic structure from the rotationally disordered rhombohedral structure might be concerted B–C exchanges [24] whose energy barriers must be of order 1 eV, and hence are kinetically suppressed at temperatures substantially below melting. This may be why the monoclinic distortion has not been observed in diffraction experiments. Likewise, thermodynamic measurements [25] primarily reveal vibrational heat capacity, with no signature of orientational ordering, because the experimental measurements are not sensitive on the required long time scales.

Owing to these experimental difficulties, first principles calculation appears to be the most promising method to resolve the thermodynamically expected low temperature ordering of boron carbide, as experiments are unlikely to achieve equilibrium. Our predicted low temperature ordering resolves fundamental questions surrounding the applicability of the third law, while our predicted high temperature structure of rhombohedral symmetry, large composition range and intrinsic disorder appears to agree satisfactorily with experiment.

Acknowledgments

We thank Yuri Grin, Nathalie Vast, Helmut Werheit and Koun Shirai for useful discussions.

References

[1] H. Okamoto, B-C (boron-carbon), J. Phase Equil. 13 (1992) 436.
[2] K.A. Schwetz, P. Karduck, Investigations of the boron-carbon system with the aid of electron probe microanalysis, J. Less Common Met. 175 (1991) 1–100.
[3] J.P. Abriata, D.E. Laughlin, The third law of thermodynamics and low temperature phase stability, Prog. Mater. Sci. 49 (2004) 367–387.
[4] H. Okamoto, T.B. Massalski, Thermodynamically improbable phase diagrams, J. Phase Equil. 12 (1991) 148–168.
[5] V. Domnich, S. Reynaud, R.A. Haber, M. Chhowalla, Boron carbide: structure properties, and stability under stress, J. Am. Ceram. Soc. 94 (2011) 3605–3628.
[6] L.B. Ekbom, C.O. Amundin, Microstructural evaluations of sintered boron carbides with different compositions, in: R. Carlsson, S. Karlsson (Eds.), Science of Ceramics, Vol. 11, Swedish Ceramic Society, 1981, pp. 273–343.
[7] V.I. Matkovich, Interstitial compounds of boron, J. Am. Ceram. Soc. 83 (1961) 1804–1806.
[8] G. Will, K.H. Kossobutzki, An x-ray structure analysis of boron carbide, b13c2, J. Less Common Met. 44 (1976) 87.
[9] G. Will, A. Kirfel, A. Gupta, E. Amberger, Electron density and bonding in B13C2, J. Less Common Met. 67 (1979) 19–29.
[10] G.H. Kwei, B. Morosin, Structures of the boron-rich boron carbides from neutron powder diffraction: implications for the nature of the inter-icosahedral chains, J. Phys. Chem. 100 (1996) 8031–8039.
[11] H.K. Clark, J.L. Hoard, The crystal structure of boron carbide, J. Am. Chem. Soc. 65 (1943) 2115–2119.
[12] G.S. Zhdanov, M.G. Sevastyanov, The crystal structure of boron carbide (b4c), Compt. Rend. Acad. Sci. U. R. S. S. 32 (1941) 432.
[13] D.M. Bylander, L. Kleinman, S. Lee, Self-consistent calculations of the energy bands and bonding properties of B13C2, Phys. Rev. B 42 (1990) 1394–1403.
[14] F. Mauri, N. Vast, C.J. Pickard, Atomic structure of icosahedral b4c boron carbide from a first principles analysis of nmr spectra, Phys. Rev. Lett. 87 (2001) 085506.
[15] R. Schmechel, H. Werheit, Structural defects of some icosahedral boron-rich solids and their correlation with the electronic properties, J. Solid State Chem. 154 (2000) 61–67.
[16] D.M. Bylander, L. Kleinman, Structure of B13C2, Phys. Rev. B 43 (1991) 1487–1491.
[17] N. Vast, J. Sjakaste, E. Betranhandy, Boron carbides from first principles, J. Phys. Conf. Ser. 176 (2009) 120002.
[18] P.E. Blöchl, Projector augmented-wave method, Phys. Rev. B 50 (1994) 17953–17979.
[19] G. Kresse, J. Hafner, *Ab initio* molecular dynamics for liquid metals, Phys. Rev. B 47 (1993) 558–561.
[20] G. Kresse, J. Furthmüller, Efficient iterative schemes for *ab initio* total energy calculations using a plane wave basis set, Phys. Rev. B 54 (1996) 11169–11186.
[21] J.P. Perdew, Atoms, molecules, solids, and surfaces: applications of the generalized gradient approximation for exchange and correlation, Phys. Rev. B 46 (1992) 6671–6687.
[22] H.J. Monkhorst, J.D. Pack, Special points for brillouin-zone integrations, Phys. Rev. B 13 (1976) 5188–5192.
[23] M. Widom, M. Mihalkovič, Symmetry-broken crystal structure of elemental boron at low temperature, Phys. Rev. B 77 (2008) 064113.
[24] R.R. Raucoules, N. Vast, E. Betranhandy, J. Sjakste, Mechanical properties of icosahedral boron carbide explained from first principles, Phys. Rev. B 84 (2011) 014112.
[25] P.A. Medwick, H.E. Fischer, R.O. Pohl, Thermal conductivity and specific heat of boron carbides, J. Alloys Compd. 203 (1994) 67–75.